Polymer 122 (2017) 270–279

Contents lists available at ScienceDirect

Polymer

journal homepage: www.elsevier.com/locate/polymer

Crystallization-driven assembly of fully degradable, natural product-based poly(L-lactide)-*block*-poly(α-D-glucose carbonate)s in aqueous solution

Yue Song, Yingchao Chen, Lu Su, Richen Li, Rachel A. Letteri, Karen L. Wooley*

Departments of Chemistry, Chemical Engineering, Materials Science & Engineering, and Laboratory for Synthetic-Biologic Interactions, Texas A&M University, P.O. Box 30012, 3255 TAMU, College Station, TX 77843, United States

ARTICLE INFO

Article history:
Received 11 May 2017
Received in revised form
21 June 2017
Accepted 24 June 2017
Available online 27 June 2017

Keywords:
Amphiphilic block copolymer
Cylindrical micelles
Crystallization-driven self assembly (CDSA)
Degradable
Natural product-based polymers

ABSTRACT

Crystallization-driven self assembly (CDSA) was achieved with fully degradable amphiphilic block polymers derived from three natural products, L-lactide, L-cysteine and D-glucose, to afford spherical and cylindrical nanostructures. A series of functional L-cysteine-modified diblock copolymers, poly(L-lactide)-*block*-poly(α-D-glucose carbonate)s (PLLA-*b*-PDGC-cys), was synthesized by organocatalyzed sequential ring-opening polymerization (ROP) of L-lactide and an alkyne-substituted bicyclic α-D-glucose carbonate, followed by UV-initiated thiol-yne "click" reaction with L-cysteine to render the PDGC block hydrophilic. Incubation of the resulting amphiphilic diblock copolymers in water at 65 °C for 30 h, followed by cooling to room temperature yielded spherical, cylindrical and 2D platelet-like bundled cylinder micellar nanostructures, depending on the PLLA weight percentage in the block copolymer, as revealed by transmission electron microscopy (TEM) and atomic force microscopy (AFM). ^{1}H NMR spectroscopy was employed to monitor the degradation of the materials over 100 d in aqueous solution at pH 1 and 10 at 37 °C, which allowed for characterization of the stability of the micelles, and for determination of the hydrolytic degradability of the polymer backbone and cleavage of the side chain moieties. Electrospray ionization (ESI) and matrix-assisted laser desorption/ionization-time of flight (MALDI-TOF) mass spectrometry were used to identify the hydrolytic degradation products of the copolymers. Overall, this work broadens the scope of CDSA to functional, natural-product based degradable block copolymers (BCPs), and the polymeric nanomaterials synthesized in this work hold promise in drug and antimicrobial delivery applications, among others.

1. Introduction

Amphiphilic block polymers are capable of self assembly into a variety of well-defined nanostructures, including spherical and cylindrical/worm-like micelles, vesicles, disks, toroids, and others [1–6], which are of great interest for applications in nanomedicine, environmental remediation and multiple other chemical industries. Cylindrical nanoparticles, in particular, have been investigated by many research groups in recent years [7–13], including significant contributions by the Müller group demonstrating the construction of cylindrical polymer brushes [14], 1D hybrid nanomaterials [15], and multi-compartment cylinders with precisely placed patches *via* hierarchical assembly of triblock terpolymer blends that have expanded the complexity and precision of block polymer solution assemblies [16–18]. The unique anisotropic and elongated shape of cylindrical nanostructures imparts notable properties, such as increased *in vivo* circulation time and altered cellular internalization pathways relative to spherical nanostructures (*i.e.,* spherical micelles and vesicles) [19–23]. Among various methods for the construction of cylindrical micelles, Manners and Winnik have pioneered crystallization-driven self assembly (CDSA) as a powerful approach yielding living epitaxial growth characteristics and, in some cases, control of length to afford nanostructures with well-defined dimensions [12,24–26]. Unlike entirely amorphous block copolymers (BCPs), solution assembly of BCPs with a crystalline block favors the formation of micellar morphologies driven by crystallization processes, which facilitate axial alignment of polymer chains and, as a result, reduced

* Corresponding author.
E-mail address: wooley@chem.tamu.edu (K.L. Wooley).

http://dx.doi.org/10.1016/j.polymer.2017.06.065
0032-3861/

interfacial curvature [13]. CDSA processes in aqueous solution have been expanded to include natural and degradable polymer components by the O'Reilly and Dove groups, in an elegant use of polylactide-containing diblock copolymers for the fabrication of nanoscopic cylinders with controlled length [11,27–30]. With our interest in polymers that are fully degradable and derived from natural products, we have now built upon the substantial recent progress in assembly of BCPs *via* CDSA [11–13,24,25,27–29,31], to explore cylindrical and spherical micelles derived from L-lactide, L-cysteine and D-glucose.

The construction of morphologically-complex nanomaterials from fully biocompatible and degradable materials synthesized from renewable resources is of broad interest as they eliminate potential environmental hazards from accumulation of non-degradable materials [32–34]. Our group has explored poly(-glucose carbonate)s, which have been receiving attention due to their potential for degradation into carbon dioxide, glucose and other small molecules [35–38]. Herein, a new type of amphiphilic BCP comprised of a zwitterionic hydrophilic poly(α-D-glucose carbonate) (PDGC) segment and a semi-crystalline hydrophobic poly(L-lactide) (PLLA) segment, was constructed by ring-opening polymerization (ROP) with a metal-free catalyst [39,40]. These diblock copolymers represent a natural product-based platform, in which both blocks are hydrolytically degradable and the PDGC segment is capable of rapid and efficient functionalization *via* the alkyne groups [41–44]. Specifically, post-polymerization modification by thiol-yne reaction with L-cysteine transformed PDGC into a hydrophilic PDGC-cys segment that afforded an overall amphiphilic character to the poly(L-lactide)-*block*-poly(α-D-glucose carbonate) (PLLA-*b*-PDGC-cys) block copolymers. Cylindrical and spherical nanostructures were obtained from aqueous solution assembly of PLLA-*b*-PDGC-cys, where spheres, cylinders and partially-reorganized 2D platelet-like bundled cylinder micellar nanostructures formed from BCPs with low, intermediate and high PLLA contents, respectively, and the hydrolytic degradability of both the PLLA and PDGC segments was confirmed through NMR spectroscopy and mass spectrometry studies.

2. Experimental section

2.1. Materials

L-Lactide was purified by recrystallization from ethyl acetate. 1,5,7-Triazabicyclo[4.4.0]dec-5-ene (TBD) was purchased from TCI chemicals. Dichloromethane (DCM) was dried using a solvent purification system (J. C. Meyer Solvent Systems, Inc., Laguna Beach, CA). Hydrochloric acid (HCl, 36.5–38.0 wt%) was purchased from Thermo-Fisher Scientific. Nanopure water (18.2 MΩ cm) was acquired from a Milli-Q water filtration system (Millipore Corp, USA). The alkyne-substituted glucose carbonate monomer, methyl-2-*O*-ethyloxycarbonyl-3-*O*-propargyloxycarbonyl-4,6-*O*-carbonyl-α-D-glucopyranoside (D-GC(EPC)), was synthesized according to a previously published procedure [36]. All other chemicals were purchased from Sigma-Aldrich (St. Louis, MO) and used without further purification unless otherwise noted. Spectra/Por dialysis membranes (MWCO 12–14 kDa) were purchased from Spectrum Laboratories, Inc. (Rancho Dominguez, CA).

2.2. Instrumentation

^{1}H NMR and ^{13}C NMR spectra were recorded on either a Varian 300 or a Varian 500 spectrometer interfaced to UNIX computers using VnmrJ software. Chemical shifts were referenced to solvent resonance signals. Fourier transform infrared (FTIR) spectra were recorded on an IR Prestige 21 system equipped with a diamond attenuated total reflection (ATR) lens (Shimadzu Corp., Japan) and analyzed using IRsolution v. 1.40 software.

Size exclusion chromatography (SEC) eluting with tetrahydrofuran (THF) was performed on a Waters Chromatography, Inc. (Milford, MA) system equipped with an isocratic pump (model 1515), a differential refractometer (model 2414), and column set comprised of a PLgel 5 μm guard column (50 × 7.5 mm), a PLgel 5 μm Mixed C column (300 × 7.5 mm, Agilent Technologies) and two Styragel® columns (500 Å and 104 Å, 300 × 7.5 mm, Waters Chromatography, Inc.). The system was operated at 40 °C with a flow rate of 1 mL/min. Data were analyzed using Breeze software from Waters Chromatography, Inc. (Milford, MA). Molecular weights were determined relative to polystyrene standards (580–3,250,000 Da) purchased from Polymer Laboratories, Inc. (Amherst, MA). Polymer solutions were prepared at a concentration of *ca.* 3 mg/mL with 0.05 vol% toluene as the flow rate marker; an injection volume of 200 μL was used.

Thermogravimetric analysis (TGA) was performed under N_2 atmosphere using a Mettler-Toledo instrument (model TGA/SDTA851e), with a heating rate of 10 °C/min, from 25 to 500 °C. Glass transition (T_g) and melting (T_m) temperatures were measured by differential scanning calorimetry (DSC) on a Mettler-Toledo DSC822® calorimeter (MettlerToledo, Inc., Columbus, OH), with a heating and cooling rate of 10 °C/min. Three heating and cooling cycles were conducted, from 30 to 165 °C for the L-cysteine-modified polymers and from 25 to 200 °C for the alkyne-functionalized polymer precursors. Measurements were analyzed using Mettler-Toledo Star^{e} v. 7.01 software. The T_g was taken as the midpoint of the inflection tangent during the second heating scan, and the T_m was taken as the maximum of the endothermic peak during the first heating scan.

Transmission electron microscopy (TEM) was performed on a FEI Tecnai F-20 electron microscope operated at 200 kV, equipped with a Gatan CCD camera. Carbon-coated copper TEM grids were pretreated with oxygen plasma to increase the surface hydrophilicity. Samples were prepared by drop-casting nanoparticle solutions (*ca.* 4 μL, 0.1 mg/mL) directly onto a grid. After 1 min, excess solution was wicked away using filter paper and the grids were allowed to dry under ambient conditions for 30 min. Uranyl acetate (1 μL, 1% aqueous solution) was then applied to the grids, which were allowed to dry in ambient conditions prior to imaging. TEM images were analyzed using ImageJ software, and 200 particles were counted from each sample to obtain the length distributions. Average nanostructure diameters were measured by counting *ca.* 50 particles.

Atomic force microscopy (AFM) was performed on a Multimode 8 system (Bruker, Santa Barbara, CA) in PeakForce Tapping® mode with ScanAsyst® image optimization software and a ScanAsyst-Air probe (k = 0.4 N/m, Bruker). Nanoparticle solutions (20 μL, 0.1 mg/mL) were deposited onto freshly cleaved mica, then excess solution was wicked away using filter paper after *ca.* 1 min and the samples were allowed to dry in ambient conditions prior to imaging. AFM images were analyzed using Nanoscope Analysis software (Bruker) to obtain the height of the nanostructures, and the average height was measured by counting 5 particles.

Wide angle X-ray diffraction (WAXD) was performed on a Bruker D8® Bragg-Brentano X-ray powder diffractometer, equipped with a 1 kW Cu tube source (1.54 Å), using an operating voltage of 40 kV and a current of 25 mA. The X-ray optics were set to standard Bragg-Brentano para-focusing mode, with X-rays focusing on the sample from an incident beam divergence-limiting slit (1 mm) and then converging onto a position-sensitive X-ray detector (Lynx-Eye, Bruker-AXS). The sample (*ca.* 10 mg) was placed in the holder of a two-circle goniometer (d = 218 mm) in a radiation safety enclosure, and standard powder θ-2θ diffraction scans were performed at

room temperature. Data collection was automated using the COMMANDER program and analyzed with EVA software (Bruker).

Electrospray ionization (ESI) mass spectrometry was performed on a Bruker amaZon SL mass spectrometer (Bruker Daltonics Inc., Billerica, MA) in both positive and negative ion modes. Matrix-assisted laser desorption/ionization-time of flight (MALDI-TOF) mass spectrometry was performed on a Voyager DE-STR mass spectrometer (Applied Biosystems, Foster City, CA) in positive linear mode. Ions were generated by a pulsed nitrogen laser (337 nm). *Trans*-2-[3-(4-*t*-butylphenyl)-2-methyl-2-propenylidene]malononitrile (DCTB) and potassium trifluoroacetate (KTFA) were used as the matrix and cationization reagent, respectively.

2.3. Synthesis and assembly of PLLA-*b*-PDGC-cys

2.3.1. Representative polymerization of L-lactide and α-D-glucose carbonate

A solution of L-lactide (77 mg, 0.54 mmol) and 4-methylbenzyl alcohol (0.1 mL, 10.9 mg/mL in DCM, 0.009 mmol) was prepared in anhydrous DCM (1.0 mL) and transferred to a vial equipped with a stir bar and a rubber septum in an argon-filled glovebox. The vial was then removed from the glovebox and connected to a Schlenk line. A solution of TBD in DCM (0.1 mL, 15.0 mg/mL, 0.01 mmol) was injected quickly into the vial of L-lactide at −78 °C. After stirring for 2 min, a solution of the glucose carbonate monomer D-GC(EPC) (200 mg, 0.535 mmol) in DCM (1.0 mL) was added *via* syringe to the reaction mixture. The reaction was stirred for an additional 10 min at −78 °C and then quenched by addition of excess acetic acid. Precipitation from DCM into methanol three times, and drying under vacuum yielded $PLLA_{45}$-*b*-$PDGC_{45}$ a white powder (215 mg, 78%). ^{1}H NMR (500 MHz, $CDCl_3$, ppm): δ 7.21 and 7.16 (AB_q, $J = 8$ Hz), 5.36 (dd, $J = 10, 10$ Hz), 5.16 (q, $J = 7$ Hz), 5.03 (d, $J = 4$ Hz), 4.89 (dd, $J = 10, 10$ Hz), 4.79–4.67 (m), 4.28 (s), 4.20 (tt, $J = 7, 4$ Hz), 4.02 (m), 3.42 (s), 2.59 (t, $J = 2$ Hz), 2.35 (s), 1.58 (d, $J = 7$ Hz), 1.30 (t, $J = 7$ Hz). ^{13}C NMR (126 MHz, $CDCl_3$, ppm): δ 169.61, 154.04, 153.63, 153.54, 129.28, 128.41, 96.41, 77.24, 76.92, 76.21, 74.12, 73.49, 72.17, 69.01, 66.63, 65.67, 64.79, 55.90, 55.76, 16.65, 14.13. FTIR: 3290, 2980, 1750, 1450, 1375, 1240, 1095, 1050, 980, 950, 880, 770, 660 cm^{-1}. SEC (THF): M_n = 14.0 kDa, $Đ$ = 1.18. T_g = 64 °C, T_m = 154 °C. TGA in Ar: 290–380 °C, 84% weight loss. The molecular weights and compositions of all polymers used in this study are provided in Table 1.

2.3.2. Representative thiol-yne click reaction of PLLA-*b*-PDGC with L-cysteine

A solution of $PLLA_{45}$-*b*-$PDGC_{45}$ (20 mg, 0.039 mmol alkyne), L-cysteine (47 mg, 0.39 mmol), HCl (0.2 mL) and 2,2-dimethoxy-2-phenylacetophenone (DMPA) (3.0 mg, 0.012 mmol) was prepared in *N*,*N*-dimethylformamide (DMF, 5 mL), deoxygenated with bubbling $N_{2(g)}$ for 5 min, and irradiated at 365 nm (1000 μJ/cm^2) for 2 h. The DMF solution was transferred into dialysis tubing (MWCO 12–14 kDa) and dialyzed against nanopure water adjusted to pH 3 with HCl at 4 °C for 36 h. The resulting solution was then lyophilized to yield the cysteine-modified polymer as a white powder. ^{1}H NMR (500 MHz, DMF-d_7, ppm): δ 7.29 and 7.21 (AB_q, $J = 8$ Hz), 5.26 (q, $J = 7$ Hz), 5.17–5.06 (m), 4.98 (br), 4.87 (br), 4.68 (br), 4.61–4.39 (m), 4.19 (br), 3.57–3.21 (m), 2.30 (s), 1.54 (d, J = 7 Hz), 1.25 (t, J = 7 Hz). ^{13}C NMR (126 MHz, DMF-d_7) δ 170.28, 170.12, 155.10, 154.81, 154.63, 129.87, 129.02, 97.09, 81.31, 72.31, 69.77, 69.14, 69.10, 68.61, 68.57, 65.71, 65.30, 65.26, 61.76, 61.70, 61.65, 61.59, 55.98, 53.43, 46.99, 20.95, 20.93, 20.87, 20.30, 17.03, 14.55, 9.06, 9.03. FTIR: 3680-2180, 1750, 1620, 1480, 1390, 1245, 1100, 1020, 880, 770, 630 cm^{-1}. T_g = 114 °C, T_m = 143 °C. TGA in Ar: 162–240 °C, 25% weight loss; 250–300 °C, 58% weight loss. All other polymers were modified with L-cysteine following the same procedure, with a molar ratio of L-cysteine: alkyne: DMPA = 10:1:0.03.

2.3.3. CDSA of PLLA-*b*-PDGC-cys diblock copolymers

PLLA-*b*-PDGC-cys was dissolved in nanopure water at concentrations between 0.05 and 0.1 mg/mL and stirred overnight at room temperature. The solutions were then heated to 65 °C for 30 h [10] to aid dissolution, and then removed from heat and allowed to cool to room temperature prior to characterization by TEM and AFM. Powder samples for WAXD experiments were obtained by lyophilization.

3. Results and discussion

3.1. Synthesis and characterization of the PLLA-*b*-PDGC-cys diblock copolymers

Sequential ROP of L-lactide and the cyclic carbonate of methyl-α-D-glucopyranoside bearing pendant ethyl- and propargyl-carbonates (D-GC(EPC)), followed by post-polymerization modification of the alkyne groups with L-cysteine yielded a series of amphiphilic diblock copolymers (PLLA-*b*-PDGC-cys, Fig. 1). The naturally-derived monomers, L-lactide and D-GC(EPC), were selected for their degradability and biocompatibility, with L-lactide providing crystallinity and D-GC(EPC) imparting functionality to the corresponding polymers [36,45]. The semi-crystalline nature of PLLA was anticipated to facilitate the formation of ordered structures, such as cylindrical micelles, while the alkyne groups of PDGC were designed to allow for versatile post-polymerization modification. Similarly as L-lactide, glucose-based cyclic carbonates are amenable to organocatalyzed ROP for the production of well-

Table 1
Characterization of the PLLA-*b*-PDGC and PLLA-*b*-PDGC-cys diblock copolymers.

	$M_{n\ NMR}$[a] (kDa)	$M_{n\ SEC}$[b] (kDa)	$Đ$[b]		M_n[c] (kDa)	M_w[d] (kDa)	PLLA (wt%)	Morphology[e]
1, $PLLA_{72}$-*b*-$PDGC_{32}$	22.3	17.3	1.08	**1′**, $PLLA_{72}$-*b*-$PDGC_{32}$-cys	30.1	32.5	34	cylinder bundles
2, $PLLA_{30}$-*b*-$PDGC_{30}$	15.6	12.7	1.12	**2′**, $PLLA_{30}$-*b*-$PDGC_{30}$-cys	22.8	25.5	19	cylinders
3, $PLLA_{45}$-*b*-$PDGC_{45}$	23.4	14.0	1.18	**3′**, $PLLA_{45}$-*b*-$PDGC_{45}$-cys	34.2	40.3	19	cylinders
4, $PLLA_{32}$-*b*-$PDGC_{52}$	24.0	16.9	1.08	**4′**, $PLLA_{32}$-*b*-$PDGC_{52}$-cys	36.6	39.5	13	cylinders
5, $PLLA_{17}$-*b*-$PDGC_{54}$	22.6	13.6	1.04	**5′**, $PLLA_{17}$-*b*-$PDGC_{54}$-cys	35.7	37.1	7	spheres
6, $PLLA_{26}$-*b*-$PDGC_{84}$	35.1	17.5	1.05	**6′**, $PLLA_{26}$-*b*-$PDGC_{84}$-cys	55.4	58.2	7	spheres
7, $PLLA_{17}$-*b*-$PDGC_{82}$	33.1	17.1	1.06	**7′**, $PLLA_{17}$-*b*-$PDGC_{82}$-cys	53.0	56.2	5	spheres

[a] Determined by ^{1}H NMR (500 MHz) in $CDCl_3$.
[b] Estimated relative to polystyrene standards by SEC eluting in THF.
[c] Calculated molecular weights from corresponding PLLA-*b*-PDGC NMR-derived molecular weights, assuming full conversion of alkyne groups.
[d] Calculated molecular weights from corresponding PLLA-*b*-PDGC NMR-derived molecular weights and SEC-derived $Đ$, assuming full conversion of alkyne groups.
[e] After self assembly in nanopure water for 30 h.

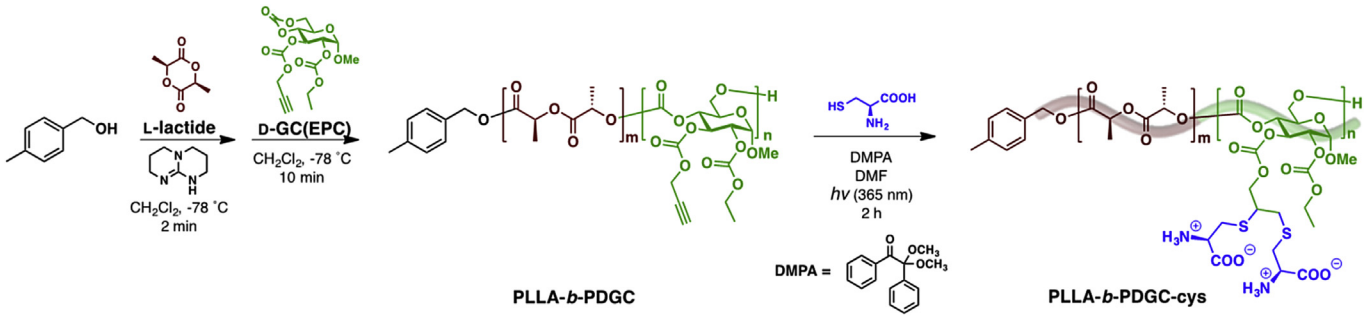

Fig. 1. Synthesis of PLLA-*b*-PDGC-cys *via* sequential ROP of L-lactide and D-GC(EPC), followed by UV-initiated thiol-yne click modification with L-cysteine.

defined polymers [35–38]. L-Lactide was polymerized first using TBD as the catalyst, which is known for mediation of high efficiency polymerization of a variety of cyclic monomers [39,46–50], and quantitative L-lactide conversion was achieved in less than 2 min. After 2–3 min, the D-GC(EPC) monomer was added to grow the PDGC block. Varying the feed ratios of the initiator and two monomers yielded PLLA-*b*-PDGC diblock copolymers **1**–**7** with different compositions and molecular weights (Table 1). Polymerizations yielding diblocks **2** and **3** employed a 1:1 M ratio of L-lactide and D-GC(EPC), and those yielding **5** and **6** employed a 1:3 M ratio of L-lactide and D-GC(EPC) to explore the effect of polymer molecular weight at constant PLLA contents on the sizes and morphologies of the resulting assemblies. FTIR, ^{1}H NMR and ^{13}C NMR spectroscopies confirmed the structures and compositions of polymers **1**–**7** (Fig. 2). ^{1}H NMR spectroscopy was also used to determine the number-average degrees of polymerization, by

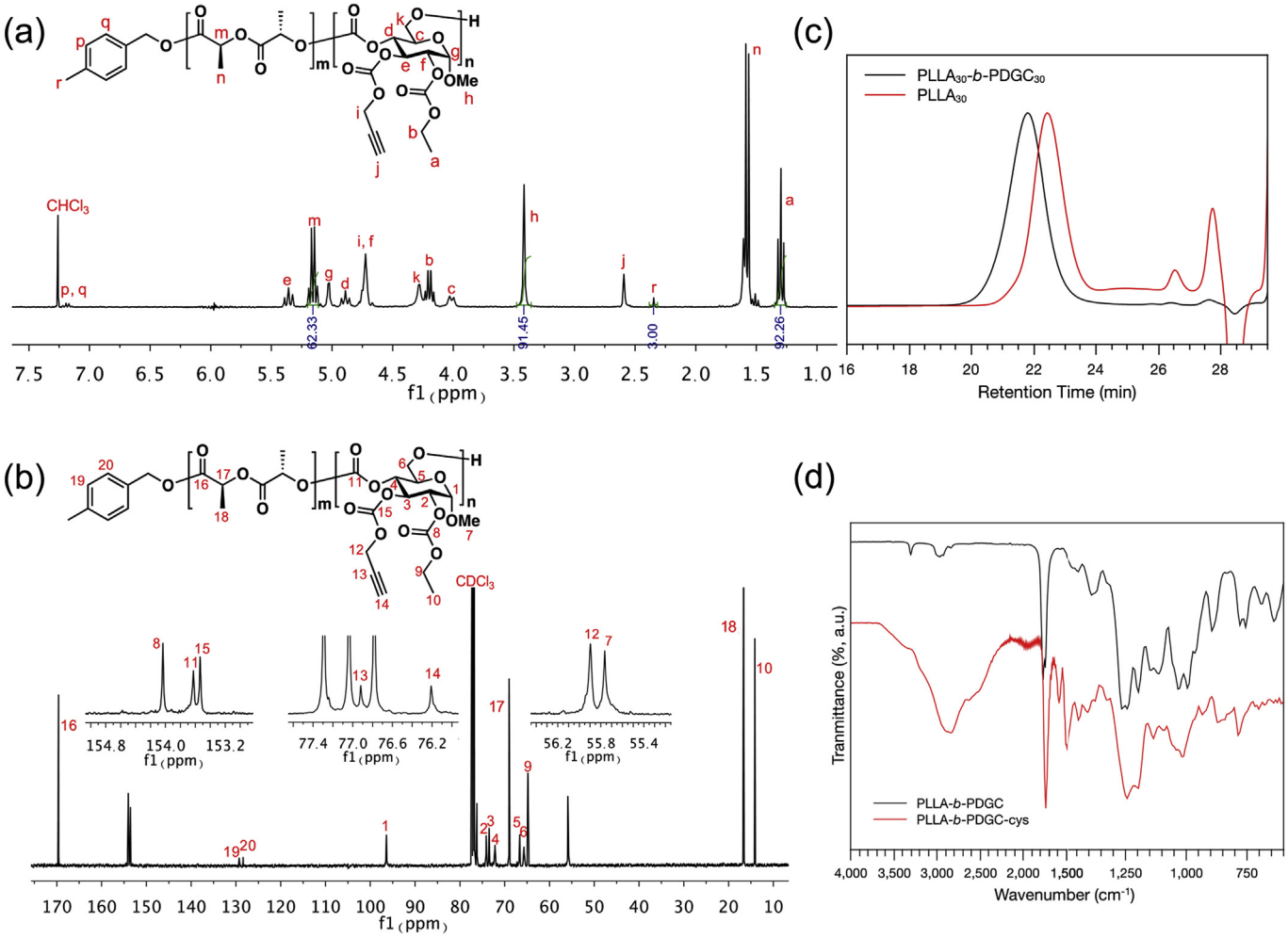

Fig. 2. Characterization of $PLLA_{30}$-*b*-$PDGC_{30}$-cys. (a) ^{1}H NMR (300 MHz) and (b) ^{13}C NMR (126 MHz) spectra acquired in $CDCl_3$. (c) SEC traces of $PLLA_{30}$-b-$PDGC_{30}$ and $PLLA_{30}$. (d) FTIR spectra of PLLA-*b*-PDGC and modified diblock copolymer PLLA-*b*-PDGC-cys.

comparing the relative integrations of peak *m* (PLLA), and *a* or *h* (PDGC) to peak *r*, corresponding to the methyl group at the polymer chain end (Fig. 2a). Narrow molecular weight distributions ($Đ < 1.20$) were observed by SEC, however, the SEC M_n values were consistently less than those derived from NMR data (Fig. 2c and Table 1), likely due to the SEC calibration against polystyrene standards.

UV-activated thiol-yne modification of the alkyne groups on the PDGC block with L-cysteine in the presence of the photoinitiator DMPA yielded amphiphilic diblock copolymers for assembly in aqueous solution. L-Cysteine was selected due to its biocompatibility and to impart a zwitterionic character to the micelle surface, which is desirable for preventing aggregation in physiological conditions and circumventing toxicity concerns associated with cationic polymers [51]. Successful addition of L-cysteine to PLLA-*b*-PDGC was achieved by employing a large excess of L-cysteine (10 equivalents relative to alkyne groups), and was supported by ^{1}H NMR spectroscopic analysis of the polymer in d_7-DMF, noting the appearance of cysteine proton resonances at δ 4.5, δ 4.2 and δ 3.4 ppm (Fig. S1). FTIR spectroscopy further revealed peaks characteristic of O-H and N-H stretching in carboxylic acid and amine groups between 3600 and 2300 cm^{-1} after modification (Fig. 2d). The overlap of these peaks with the characteristic alkyne C-H stretching peak at *ca.* 3300 cm^{-1} complicated IR analysis of alkyne consumption, however the disappearance of the carbon resonances of the alkyne groups at δ 76.20 and 76.93 ppm indicated full conversion of the alkyne residues to thioether linkages (Fig. S1), consistent with quantitative conversion of alkyne moieties observed in similar reactions of cysteine, cysteamine, and 3-mercaptopropionic acid with other alkyne-containing polyphosphoester (PPE)-, PLLA- and PDGC-containing diblock copolymers [35,52,53]. Additionally, TGA indicated a two-stage decomposition, with mass loss measured between 140-162 °C and 250–300 °C (Fig. S2), corresponding to the loss of cysteine moieties and the decomposition of polymer backbone, respectively, and agreeing well with the polymer compositions determined by NMR spectroscopy. For instance, TGA of PLLA$_{45}$-*b*-PDGC$_{45}$-cys measured 27% mass loss between 162 and 240 °C and 58% mass loss between 250 and 300 °C (Fig. S2). Across the series of PLLA$_m$-*b*-PDGC$_n$-cys, the percentage mass loss at the lower temperature range (162–240 °C) increased as the value of n/m increased. Taken together, the NMR, SEC, FTIR and TGA data indicate the successful synthesis of a series of well-defined amphiphilic diblock copolymers amenable to crystallization-driven assembly in aqueous solution, enabling exploration of the effects of composition, molecular weight, and crystallinity on solution assembly behavior.

3.2. Crystallization-driven assembly of PLLA-b-PDGC-cys

To investigate the crystallization-driven assembly of PLLA-*b*-PDGC-cys, polymer solutions (0.05–0.1 mg/mL) were heated in nanopure water for 30 h [10] at 65 °C to raise the solution temperature above the T_g of PLLA to aid dissolution, and then removed from heat and cooled to room temperature (Fig. 3). The resulting assemblies were characterized by TEM and AFM.

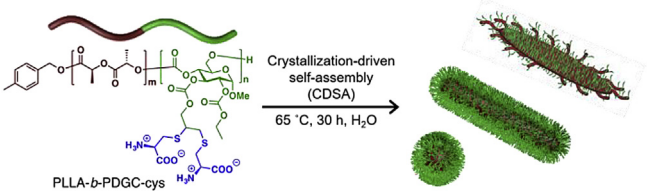

Fig. 3. Crystallization-driven assembly of PLLA-*b*-PDGC-cys BCPs in aqueous solution into spherical, cylindrical, and 2D platelet-like bundled cylindrical nanostructures.

3.2.1. PLLA-b-PDGC-cys nanostructure characterization by TEM and AFM

Following crystallization-driven assembly, TEM and AFM images (Fig. 4) revealed spherical, cylindrical and 2D platelet-like bundled cylindrical micellar morphologies, depending on the weight percentage of PLLA in the diblock copolymers. The diblock copolymer with the highest PLLA weight percentage (34 wt%, polymer **1′**, Fig. S6) yielded what appeared to be bundles of cylindrical nanostructures that were assembled into 2D platelets having average heights of 12 ± 2 nm, attributed to insufficient coronal repulsion. In contrast, strong repulsion between the hydrophilic PDGC-cys chains of polymers with low hydrophobic contents (<13 wt% PLLA, polymers **5′**-**7′**) promoted the formation of spherical micelles with high interfacial curvature upon aqueous crystallization-driven assembly. Polymers **2′**-**4′** with intermediate hydrophobic contents (13–19 wt% PLLA) assembled into cylinders with diameters ranging from 19 to 30 nm and a broad distribution of lengths (Fig. 4b–d); the distribution histograms are provided in Fig. S4. Micelle dimensions were obtained using lengths and diameters measured from the TEM micrographs, while the heights were measured from AFM images. Polymers **2′** and **3′,** synthesized with 19 wt% PLLA and different molecular weights (22.8 and 34.2 kDa overall, with PLLA DP$_n$ values of 30 and 45, respectively) yielded cylinders with diameters of 21 ± 1 nm and 30 ± 3 nm, respectively. The assembly behaviors observed with these naturally-derived amphiphilic diblock copolymers are consistent with previously published results for poly(acrylic acid) (PAA)-*b*-PLLA assemblies, where cylinders formed following crystallization-driven assembly in water from diblock copolymers with hydrophobic fractions exceeding 18 wt% and spherical micelles formed from polymers with lower hydrophobic fractions [27]. It is interesting that the number-averaged height of the bundled cylinders of polymer **1'** (12 ± 2 nm) was significantly less that the heights of the cylinders of **2′** and **3'** (18 ± 2 nm and 19 ± 2 nm) (Fig. S6), even though the PLLA degree of polymerization was greater (72 *vs*. 30 *vs*. 45, respectively), which suggests partial reorganization and co-crystallization between the cores of individual cylinders. Further studies are underway to investigate these phenomena and gain control over the length and dispersity of the resulting nanostructures obtained from crystallization-driven assembly of these degradable amphiphilic diblock copolymers.

3.2.2. WAXD characterization of PLLA-b-PDGC-cys

To determine the crystallinity of nanostructures formed following CDSA, WAXD was performed on assemblies of polymers **1′**, **2′, 4′**, **6′**, and **7'** (Fig. 5). The presence of the characteristic diffractions at 2θ = 16.6° and 19.1°, corresponding to the diffractions of (110)/(200) and (203) of the PLLA domains, respectively [10,27,54], verified the crystalline nature of the micelle cores. The intensity of the peak decreased with decreasing PLLA weight fraction in the diblock copolymers, wherein WAXD of the cylindrical nanostructures formed from polymers **1′**, **2′** and **4′** showed an obvious peak, while almost no peak was observed for the spherical micelles formed from polymers **6′** and **7′**, having the lowest PLLA weight contents. These WAXD results provide strong evidence of the key influence of crystallization in the self assembly process.

3.3. Hydrolytic degradation of PLLA-b-PDGC-cys

The ester and carbonate linkages of the PLLA and PDGC backbone segments, respectively, can be cleaved by spontaneous

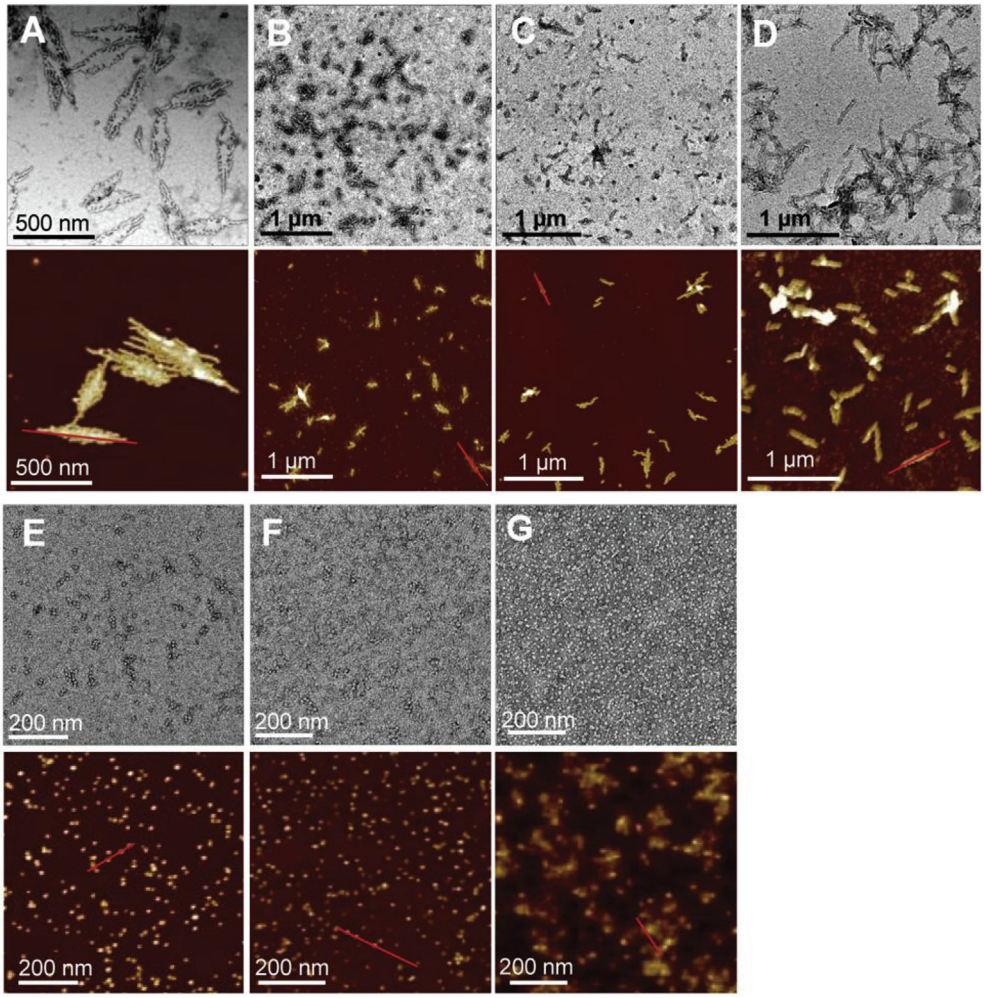

Fig. 4. TEM micrographs (top) and AFM images (bottom) of assemblies from PLLA-*b*-PDGC-cys following crystallization-driven assembly. (A) Bundled cylinder platelets assembled from $PLLA_{72}$-*b*-$PDGC_{32}$-cys, **polymer 1'**. (B) Cylinders assembled from $PLLA_{30}$-*b*-$PDGC_{30}$-cys, **polymer 2'**: diameter (d) = 21 ± 1 nm. (C) Cylinders assembled from $PLLA_{45}$-*b*-$PDGC_{45}$-cys, **polymer 3'**: d = 30 ± 3 nm. (D) Cylinders assembled from $PLLA_{32}$-*b*-$PDGC_{52}$-cys, **polymer 4'**: d = 23 ± 1 nm. (E) Spheres assembled from $PLLA_{17}$-*b*-$PDGC_{54}$-cys, **polymer 5'**: d = 15 ± 1 nm. (F) Spheres assembled from $PLLA_{26}$-*b*-$PDGC_{84}$-cys, **polymer 6'**: d = 13 ± 1 nm. (G) Spheres assembled from $PLLA_{17}$-*b*-$PDGC_{82}$-cys, **polymer 7'**: d = 14 ± 2 nm.

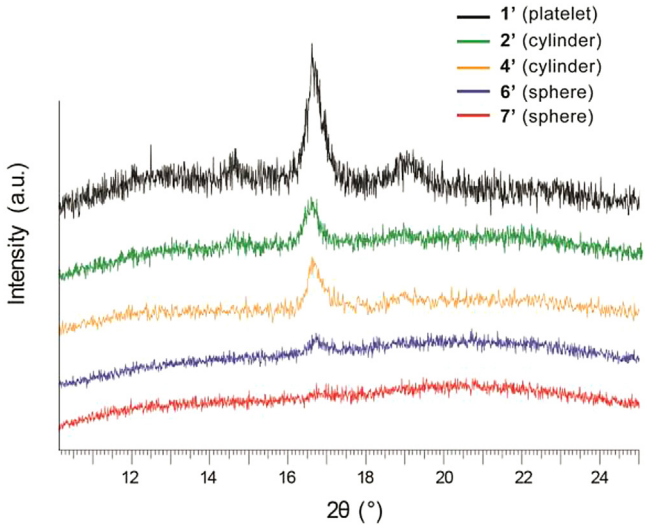

Fig. 5. WAXD diffractograms of the nanostructures from polymers **1′**, **2′**, **4′**, **6′**, and **7′**. The peaks at 2θ = 16.6° and 19.1° correspond to the diffractions of (110)/(200) and (203) within crystalline regions of the PLLA nanostructure cores, respectively.

hydrolysis and/or enzymatic degradation [55–57]. Hydrolytic degradation of diverse polymers has been studied previously using NMR spectroscopy [57,58], SEC [58], dynamic light scattering (DLS) [57] and mass spectrometry [57]. In this work, the stability of the PLLA-*b*-PDGC-cys diblock copolymers was evaluated in aqueous solutions (pH 1 and 10) at 37 °C over 100 d by monitoring changes in the ^{1}H NMR spectra at δ 4.50–3.70, 3.50–2.50 and 1.13 ppm, corresponding to the proton resonances of L-cysteine-related moieties and D-glucose carbonate degradation products, and at δ 1.37 and 3.60 ppm, corresponding to L-lactide degradation products (Fig. 6). Following NMR-based hydrolytic degradation studies, the solutions were analyzed by ESI and MALDI-TOF mass spectrometries (Fig. 7).

3.3.1. Degradation of PLLA-b-PDGC-cys in aqueous solutions monitored by ^{1}H NMR spectroscopy

The PLLA-*b*-PDGC-cys diblock copolymers contain ester linkages in the PLLA segments and carbonate linkages in the PDGC-cys segments, which are potentially hydrolytically degradable. To evaluate the degradation of the ester and carbonate linkages along the polymer backbone and side chains, aqueous solutions (D_2O) in NMR tubes containing *ca.*5 mg/mL of PLLA-*b*-PDGC-cys **6′** at pH 1

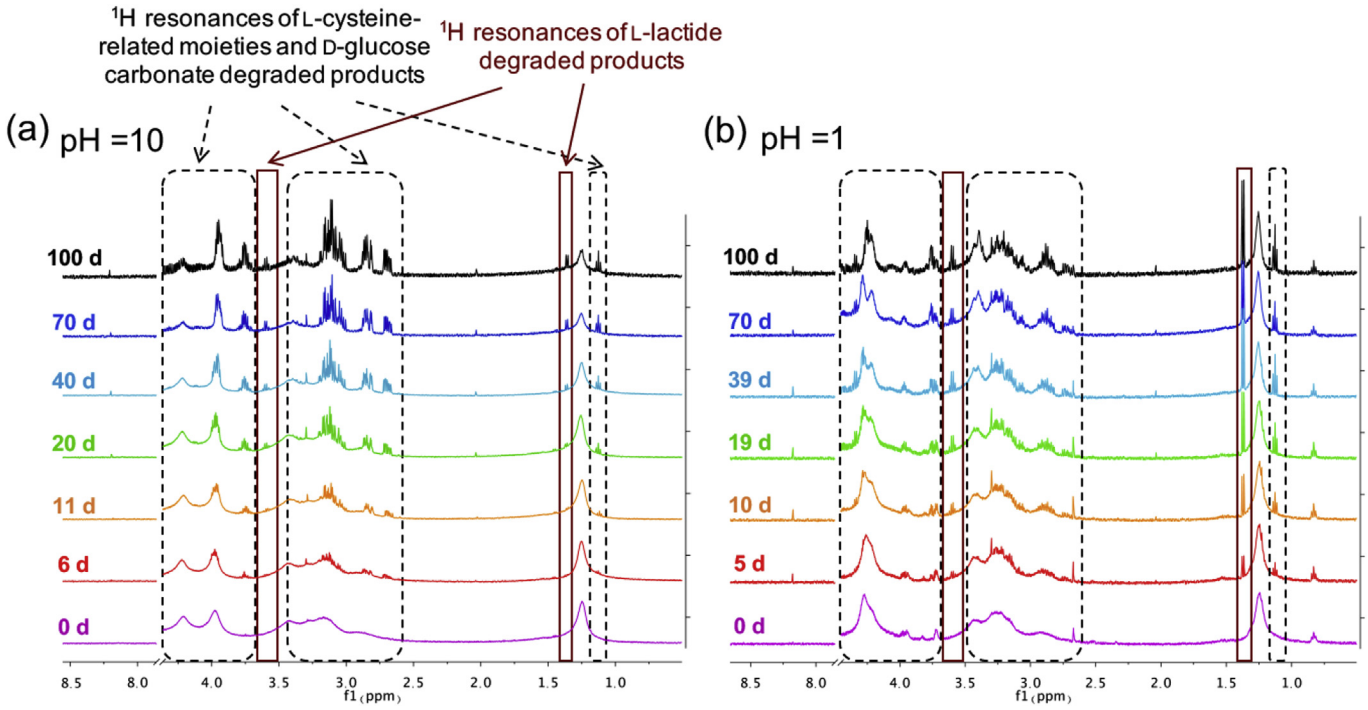

Fig. 6. ^{1}H NMR (500 MHz) spectra of PLLA-*b*-PDGC-cys **6′** acquired in D_2O (ca. 5 mg/mL) adjusted to pH 10 (a) and 1 (b) during incubation at 37 °C over 100 d.

and 10 were incubated at 37 °C, and degradation profiles were measured by ^{1}H NMR spectroscopy over 100 d. For each pH condition, sharp peaks appeared and increased in intensity with time, attributed to the production of small molecules and oligomers during polymer degradation (Fig. 6). Specifically, the doublet at δ 1.37 ppm and the quartet at δ 3.60 ppm are attributed to the ^{1}H resonances of the degradation products of the PLLA segment, whereas the multiplets at δ 4.50–3.70, 3.50–2.65 ppm and the triplet at δ 1.13 ppm are attributed to hydrolytic degradation of the PDGC backbone and side chain carbonate linkages into glucose- and cysteine-based small molecules. Up- and down-field shifts of proton resonances corresponding to different protonation states of the carboxylic acid and amine groups of cysteine explain some of the differences between spectra acquired at pH 1 and pH 10. Precipitation of the polymer within 1 d upon incubation at 37 °C in aqueous solutions at either pH 7.4 (1× phosphate buffered saline) or pH 5.0 (sodium acetate/acetic acid buffer), attributed to interactions between the protonated amine and deprotonated carboxylic groups under neutral conditions, prevented the ability to conduct degradation studies at neutral pH [59]. Nevertheless, these NMR studies confirmed the hydrolytic degradability of both segments of these amphiphilic diblock copolymers that were demonstrated to undergo CDSA into a variety of nanostructures.

3.3.2. Identification of PLLA-b-PDGC-cys degradation products by ESI mass spectrometry

The degradation products of the PLLA-*b*-PDGC-cys diblock copolymer **6′** were identified using ESI (Fig. 7) and MALDI-TOF (Fig. S5) mass spectrometric analyses, following incubation at 37 °C in D_2O (*ca.* 5 mg/mL) adjusted to pH 1 and 10 for 100 d. By 100 d, the integration of the sharp peaks in the ^{1}H NMR spectra corresponding to small molecule degradation products no longer increased obviously in intensity. The hydrolytic degradation data in Fig. 7 suggest that the PDGC-cys segment was hydrolyzed into small molecules as the carbonate linkages in the PDGC backbone and side chains broke down, yielding methyl D-glucopyranoside and L-cysteine-related moieties. The hydrolytic degradability of the ester linkages of PLLA was confirmed by the presence of ESI mass spectrometry signals corresponding to the unimer and dimer of lactic acid (**a** and **b** in Fig. 7b), as well as of oligomers with a distribution of regularly spaced peaks at intervals of *m*/*z* 72 Da (corresponding to the molecular weight of a PLLA repeat unit). Two distributions of lactic acid oligomer peaks were observed, corresponding to oligomers with and without 4-methylbenzyl alcohol end groups. Finally, MALDI-TOF analysis of the mixture of degradation products confirmed the degradation of the polymers into small molecules and oligomers by the disappearance of high molecular weight peaks and appearance of lower molecular weight peaks (Fig. S5).

4. Conclusions

In summary, fully degradable, well-defined functional amphiphilic diblock copolymers synthesized from natural products were demonstrated to undergo crystallization-driven assembly in aqueous solution into a variety of nanostructures. Well-defined diblock copolymers with alkyne-containing side chains were prepared by TBD-catalyzed sequential ROP of L-lactide and a bicyclic alkyne-substituted glucose carbonate. Subsequent modification of the alkyne side chain moieties with L-cysteine in a highly efficient UV-initiated thiol-yne reaction afforded amphiphilic semi-crystalline diblock copolymers with controlled molecular weights and compositions. Crystallization-driven assembly of the resulting polymers in aqueous solution afforded a series of nanoparticles, of which the morphology varied with PLLA content. AFM and TEM confirmed the successful formation of spherical and cylindrical nanostructures from PLLA-*b*-PDGC-cys. Importantly, the degradability of these micellar nanoparticles was demonstrated in comprehensive degradation studies involving ^{1}H NMR spectroscopy, and ESI and MALDI-TOF mass spectrometry measurements.

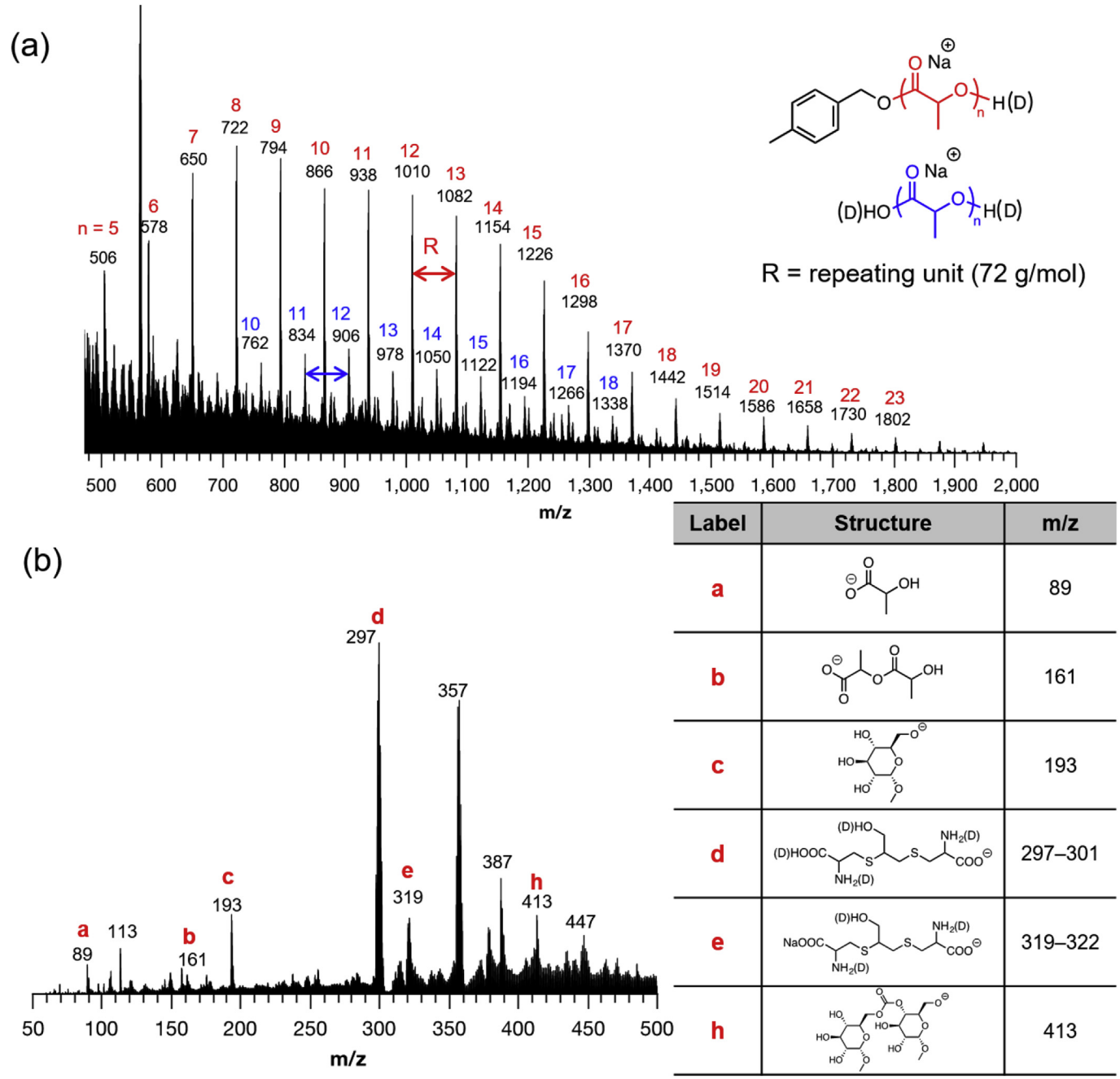

Label	Structure	m/z
a		89
b		161
c		193
d		297–301
e		319–322
h		413

Fig. 7. ESI MS analysis of the degradation products of the polymer **6'**. Mass spectra acquired in positive ion mode, *m*/*z* range of 500–2000 (a), and in negative ion mode, *m*/*z* range of 50–500 (b).

Assembly procedures yielding control over nanostructure dimensions, and encapsulation and release of therapeutic agents using these functional, degradable micelles are under investigation.

Acknowledgements

This material is based upon work supported by the National Science Foundation (CHE-1610311, DMREF-1629094, and DMR-1507429). We also gratefully acknowledge financial support from the Robert A. Welch Foundation through the W. T. Doherty-Welch Chair in Chemistry (A-0001). Dr. Bo Wang is acknowledged for obtaining the mass spectrometry data, and Dr. Joseph H. Reibenspies for the WAXD analysis.

Appendix A. Supplementary data

Supplementary data related to this article can be found at http://dx.doi.org/10.1016/j.polymer.2017.06.065.

References

[1] S. Jain, F.S. Bates, On the origins of morphological complexity in block copolymer surfactants, Science 300 (5618) (2003) 460–464.

[2] S.J. Holder, N.A.J.M. Sommerdijk, New micellar morphologies from amphiphilic block copolymers: disks, toroids and bicontinuous micelles, Polym. Chem. 2 (5) (2011) 1018–1028.
[3] A. Blanazs, J. Madsen, G. Battaglia, A.J. Ryan, S.P. Armes, Mechanistic insights for block copolymer morphologies: how do worms form vesicles? J. Am. Chem. Soc. 133 (41) (2011) 16581–16587.
[4] H. Qiu, Z.M. Hudson, M.A. Winnik, I. Manners, Multidimensional hierarchical self-assembly of amphiphilic cylindrical block comicelles, Science 347 (6228) (2015) 1329–1332.
[5] Y. Mai, A. Eisenberg, Self-assembly of block copolymers, Chem. Soc. Rev. 41 (18) (2012) 5969–5985.
[6] F. Zhang, S. Zhang, S.F. Pollack, R. Li, A.M. Gonzalez, J. Fan, J. Zou, S.E. Leininger, A. Pavia-Sanders, R. Johnson, L.D. Nelson, J.E. Raymond, M. Elsabahy, D.M. Hughes, M.W. Lenox, T.P. Gustafson, K.L. Wooley, Improving paclitaxel delivery: in vitro and in vivo characterization of PEGylated polyphosphoester-based nanocarriers, J. Am. Chem. Soc. 137 (5) (2015) 2056–2066.
[7] J. Chai, J.M. Buriak, Using cylindrical domains of block copolymers to self-assemble and align metallic nanowires, ACS Nano 2 (3) (2008) 489–501.
[8] L. Sun, A. Pitto-Barry, A.W. Thomas, M. Inam, K. Doncom, A.P. Dove, R.K. O'Reilly, Core functionalization of semi-crystalline polymeric cylindrical nanoparticles using photo-initiated thiol-ene radical reactions, Polym. Chem. 7 (13) (2016) 2337–2341.
[9] M. Zhang, A.H.E. Müller, Cylindrical polymer brushes, J. Polym. Sci. Part A Polym. Chem. 43 (16) (2005) 3461–3481.
[10] N. Petzetakis, D. Walker, A.P. Dove, R.K. O'Reilly, Crystallization-driven sphere-to-rod transition of poly(lactide)-b-poly(acrylic acid) diblock copolymers: mechanism and kinetics, Soft Matter 8 (28) (2012) 7408–7414.
[11] N. Petzetakis, A.P. Dove, R.K. O'Reilly, Cylindrical micelles from the living crystallization-driven self-assembly of poly (lactide)-containing block copolymers, Chem. Sci. 2 (5) (2011) 955–960.
[12] X. Wang, G. Guerin, H. Wang, Y. Wang, I. Manners, M.A. Winnik, Cylindrical block copolymer micelles and Co-Micelles of controlled length and architecture, Science 317 (5838) (2007) 644–647.
[13] J.B. Gilroy, T. Gädt, G.R. Whittell, L. Chabanne, J.M. Mitchels, R.M. Richardson, M.A. Winnik, I. Manners, Monodisperse cylindrical micelles by crystallization-driven living self-assembly, Nat. Chem. 2 (7) (2010) 566–570.
[14] M. Müllner, A.H. Müller, Cylindrical polymer brushes–anisotropic building blocks, unimolecular templates and particulate nanocarriers, Polymer 98 (2016) 389–401.
[15] J. Yuan, A.H. Müller, One-dimensional organic–inorganic hybrid nanomaterials, Polymer 51 (18) (2010) 4015–4036.
[16] T.I. Löbling, O. Borisov, J.S. Haataja, O. Ikkala, A.H. Gröschel, A.H.E. Müller, Rational design of ABC triblock terpolymer solution nanostructures with controlled patch morphology, Nat. Commun. 7 (2016) 12097.
[17] A.H. Groschel, A. Walther, T.I. Lobling, F.H. Schacher, H. Schmalz, A.H.E. Muller, Guided hierarchical co-assembly of soft patchy nanoparticles, Nature 503 (7475) (2013) 247–251.
[18] A.H. Gröschel, F.H. Schacher, H. Schmalz, O.V. Borisov, E.B. Zhulina, A. Walther, A.H.E. Müller, Precise hierarchical self-assembly of multicompartment micelles, Nat. Commun. 3 (2012) 710.
[19] Y. Geng, P. Dalhaimer, S. Cai, R. Tsai, M. Tewari, T. Minko, D.E. Discher, Shape effects of filaments versus spherical particles in flow and drug delivery, Nat. Nanotechnol. 2 (4) (2007) 249–255.
[20] K. Zhang, H. Fang, Z. Chen, J.-S.A. Taylor, K.L. Wooley, Shape effects of nanoparticles conjugated with cell-penetrating peptides (HIV tat PTD) on CHO cell uptake, Bioconjugate Chem. 19 (9) (2008) 1880–1887.
[21] A. Harada, K. Kataoka, Supramolecular assemblies of block copolymers in aqueous media as nanocontainers relevant to biological applications, Progr. Polym. Sci. 31 (11) (2006) 949–982.
[22] E. Hinde, K. Thammasiraphop, H.T. Duong, J. Yeow, B. Karagoz, C. Boyer, J.J. Gooding, K. Gaus, Pair correlation microscopy reveals the role of nanoparticle shape in intracellular transport and site of drug release, Nat. Nanotechnol. 12 (1) (2017) 81–89.
[23] N.S. Lee, L.Y. Lin, W.L. Neumann, J.N. Freskos, A. Karwa, J.J. Shieh, R.B. Dorshow, K.L. Wooley, Influence of nanostructure morphology on host capacity and kinetics of guest release, Small 7 (14) (2011) 1998–2003.
[24] J.A. Massey, K. Temple, L. Cao, Y. Rharbi, J. Raez, M.A. Winnik, I. Manners, Self-assembly of organometallic block copolymers: the role of crystallinity of the core-forming polyferrocene block in the micellar morphologies formed by poly(ferrocenylsilane-b-dimethylsiloxane) in n-alkane solvents, J. Am. Chem. Soc. 122 (47) (2000) 11577–11584.
[25] G. Cambridge, M.J. Gonzalez-Alvarez, G. Guerin, I. Manners, M.A. Winnik, Solution self-assembly of blends of crystalline-coil polyferrocenylsilane-block-polyisoprene with crystallizable polyferrocenylsilane homopolymer, Macromolecules 48 (3) (2015) 707–716.
[26] J.J. Crassous, P. Schurtenberger, M. Ballauff, A.M. Mihut, Design of block copolymer micelles via crystallization, Polymer 62 (2015) A1–A13.
[27] L. Sun, N. Petzetakis, A. Pitto-Barry, T.L. Schiller, N. Kirby, D.J. Keddie, B.J. Boyd, R.K. O'Reilly, A.P. Dove, Tuning the size of cylindrical micelles from poly(l-lactide)-b-poly(acrylic acid) diblock copolymers based on crystallization-driven self-assembly, Macromolecules 46 (22) (2013) 9074–9082.
[28] A. Pitto-Barry, N. Kirby, A.P. Dove, R.K. O'Reilly, Expanding the scope of the crystallization-driven self-assembly of polylactide-containing polymers, Polym. Chem. 5 (4) (2014) 1427–1436.
[29] L. Sun, A. Pitto-Barry, N. Kirby, T.L. Schiller, A.M. Sanchez, M.A. Dyson, J. Sloan, N.R. Wilson, R.K. O'Reilly, A.P. Dove, Structural reorganization of cylindrical nanoparticles triggered by polylactide stereocomplexation, Nat. Commun. 5 (2014) 5746.
[30] M. Inam, G. Cambridge, A. Pitto-Barry, Z.P.L. Laker, N.R. Wilson, R.T. Mathers, A.P. Dove, R.K. O'Reilly, 1D vs. 2D shape selectivity in the crystallization-driven self-assembly of polylactide block copolymers, Chem. Sci. 8 (2017) 4223–4230.
[31] J. Wang, W. Zhu, B. Peng, Y. Chen, A facile way to prepare crystalline platelets of block copolymers by crystallization-driven self-assembly, Polymer 54 (25) (2013) 6760–6767.
[32] W.C. Shearouse, L.M. Lillie, T.M. Reineke, W.B. Tolman, Sustainable polyesters derived from glucose and Castor oil: building block structure impacts properties, ACS Macro Lett. 4 (3) (2015) 284–288.
[33] M.A. Hillmyer, W.B. Tolman, Aliphatic polyester block polymers: renewable, degradable, and sustainable, Acc. Chem. Res. 47 (8) (2014) 2390–2396.
[34] S.A. Miller, Sustainable polymers: opportunities for the next decade, ACS Macro Lett. 2 (6) (2013) 550–554.
[35] T.P. Gustafson, A.T. Lonnecker, G.S. Heo, S. Zhang, A.P. Dove, K.L. Wooley, Poly(d-glucose carbonate) block copolymers: a platform for natural product-based nanomaterials with solvothermatic characteristics, Biomacromolecules 14 (9) (2013) 3346–3353.
[36] L. Su, S. Khan, J.W. Fan, Y.N. Lin, H. Wang, T.P. Gustafson, F.W. Zhang, K.L. Wooley, Functional sugar-based polymers and nanostructures comprised of degradable poly(D-glucose carbonate)s, Polym. Chem. 8 (10) (2017) 1699–1707.
[37] K. Mikami, A.T. Lonnecker, T.P. Gustafson, N.F. Zinnel, P.-J. Pai, D.H. Russell, K.L. Wooley, Polycarbonates derived from glucose via an organocatalytic approach, J. Am. Chem. Soc. 135 (18) (2013) 6826–6829.
[38] D. Pati, X. Feng, N. Hadjichristidis, Y. Gnanou, Hydrophobic, hydrophilic, and amphiphilic polyglycocarbonates with linear and macrocyclic architectures from bicyclic glycocarbonates derived from CO_2 and glucoside, Macromolecules 50 (4) (2017) 1362–1370.
[39] R.C. Pratt, B.G. Lohmeijer, D.A. Long, R.M. Waymouth, J.L. Hedrick, Triazabicyclodecene: a simple bifunctional organocatalyst for acyl transfer and ring-opening polymerization of cyclic esters, J. Am. Chem. Soc. 128 (14) (2006) 4556–4557.
[40] M.K. Kiesewetter, E.J. Shin, J.L. Hedrick, R.M. Waymouth, Organocatalysis: opportunities and challenges for polymer synthesis, Macromolecules 43 (5) (2010) 2093–2107.
[41] L. Liang, D. Astruc, The copper (I)-catalyzed alkyne-azide cycloaddition (CuAAC)"click" reaction and its applications. An overview, Coord. Chem. Rev. 255 (23) (2011) 2933–2945.
[42] C.E. Hoyle, C.N. Bowman, Thiol–ene click chemistry, Angew. Chem. Int. Ed. 49 (9) (2010) 1540–1573.
[43] A.B. Lowe, C.E. Hoyle, C.N. Bowman, Thiol-yne click chemistry: a powerful and versatile methodology for materials synthesis, J. Mater. Chem. 20 (23) (2010) 4745–4750.
[44] U. Halbes-Letinois, J.-M. Weibel, P. Pale, The organic chemistry of silver acetylides, Chem. Soc. Rev. 36 (5) (2007) 759–769.
[45] Y. Kikkawa, H. Abe, T. Iwata, Y. Inoue, Y. Doi, Crystallization, stability, and enzymatic degradation of poly(l-lactide) thin film, Biomacromolecules 3 (2) (2002) 350–356.
[46] M.K. Kiesewetter, M.D. Scholten, N. Kirn, R.L. Weber, J.L. Hedrick, R.M. Waymouth, Cyclic guanidine organic catalysts: what is magic about triazabicyclodecene? J. Org. Chem. 74 (24) (2009) 9490–9496.
[47] Y.-Y.T. Tsao, K.L. Wooley, Synthetic, functional thymidine-derived polydeoxyribonucleotide analogues from a six-membered cyclic phosphoester, J. Am. Chem. Soc. 139 (15) (2017) 5467–5473.
[48] S. Zhang, H. Wang, Y. Shen, F. Zhang, K. Seetho, J. Zou, J.S. Taylor, A.P. Dove, K.L. Wooley, A simple and efficient synthesis of an acid-labile polyphosphoramidate by organobase-catalyzed ring-opening polymerization and transformation to polyphosphoester ionomers by acid treatment, Macromolecules 46 (13) (2013) 5141–5149.
[49] E.A. Appel, V.Y. Lee, T.T. Nguyen, M. McNeil, F. Nederberg, J.L. Hedrick, W.C. Swope, J.E. Rice, R.D. Miller, J. Sly, Toward biodegradable nanogel star polymers via organocatalytic ROP, Chem. Commun. 48 (49) (2012) 6163–6165.
[50] C.G. Jaffredo, J.-F. Carpentier, S.M. Guillaume, Organocatalyzed controlled ROP of [small beta]-lactones towards poly(hydroxyalkanoate)s: from [small beta]-butyrolactone to benzyl [small beta]-malolactone polymers, Polym. Chem. 4 (13) (2013) 3837–3850.
[51] A.B. Lowe, C.L. McCormick, Synthesis and solution properties of zwitterionic polymers, Chem. Rev. 102 (11) (2002) 4177–4190.
[52] S. Zhang, J. Zou, F. Zhang, M. Elsabahy, S.E. Felder, J. Zhu, D.J. Pochan, K.L. Wooley, Rapid and versatile construction of diverse and functional nanostructures derived from a polyphosphoester-based biomimetic block copolymer system, J. Am. Chem. Soc. 134 (44) (2012) 18467–18474.
[53] Y.H. Lim, G.S. Heo, S. Cho, K.L. Wooley, Construction of a reactive diblock copolymer, polyphosphoester–poly(L-lactide), as a versatile framework for functional materials that are capable of full degradation and nanoscopic assembly formation, ACS Macro Lett. 2 (9) (2013) 785–789.
[54] W. Wang, H. Qi, T. Zhou, S. Mei, L. Han, T. Higuchi, H. Jinnai, C.Y. Li, Highly robust crystalsome via directed polymer crystallization at curved liquid/liquid interface, Nat. Commun. 7 (2016) 10599.
[55] Y. Tokiwa, B.P. Calabia, C.U. Ugwu, S. Aiba, Biodegradability of plastics, Int. J.

Mol. Sci. 10 (9) (2009) 3722–3742.
[56] D. Garlotta, A literature review of poly(lactic acid), J. Polym. Environ. 9 (2) (2001) 63–84.
[57] Y.H. Lim, K.M. Tiemann, G.S. Heo, P.O. Wagers, Y.H. Rezenom, S. Zhang, F. Zhang, W.J. Youngs, D.A. Hunstad, K.L. Wooley, Preparation and in vitro antimicrobial activity of silver-bearing degradable polymeric nanoparticles of polyphosphoester-block-poly(l-lactide), ACS Nano 9 (2) (2015) 1995–2008.
[58] H. Wang, L. Su, R. Li, S. Zhang, J. Fan, F. Zhang, T.P. Nguyen, K.L. Wooley, Polyphosphoramidates that undergo acid-triggered backbone degradation, ACS Macro Lett. 6 (3) (2017) 219–223.
[59] H. Akbulut, S. Yamada, T. Endo, Preparation of a zwitterionic polymer based on l-cysteine for recovery application of precious metals, RSC Adv. 6 (110) (2016) 108689–108696.